Effects of an intervening airgap on the two fundamental modes of a surface waveguide

M.V. Andres, DSc
Prof. V. Such, DSc

Indexing terms: *Waveguides, Transmission lines*

Abstract: The introduction of an intervening airgap in a circular surface waveguide is investigated. The radial field structure and the propagation characteristics of the two fundamental modes are shown, as well as their dependence on the airgap and the frequency. The thickness of the airgap is a new parameter that might be used to improve the propagation characteristics of the surface waveguide as a low-loss transmission line, or to control the penetration of the fields in the surrounding medium, allowing a design of the waveguide as a leaky transmission line.

List of principal symbols

ρ, ϕ, z	= cylindrical co-ordinates
a, b, c	= radii of the waveguide
λ_0, k_0	= wavelength and wavenumber in the vacuum
β	= axial propagation factor
α_d	= attenuation factor due to the losses in the dielectric medium
h, k	= radial propagation factors in the air and in the dielectric medium
x, y	= normalised radial propagation factors
$\varepsilon_r, \mu_r, \tan\delta$	= relative permittivity, relative permeability and loss tangent of the dielectric medium
f_0	= normalised frequency
J_n, Y_n, I_n, K_n	= Bessel functions and modified Bessel functions of first and second kind of order n
j	$= \sqrt{-1}$
Γ	= 1.78107
P_1, P_2, P_3	= relative contributions to the power flow of each medium
RECS	= radius of the effective cross-section

1 Introduction

The introduction of an intervening airgap has been investigated in different structures. It has been shown that such airgaps can reduce the attenuation of a closed waveguide [1, 2]. The advantages of these airgaps have also been investigated in the diffraction and scattering of opened structure [3, 4]. We wish to show the effects that an airgap can have on the propagation characteristics of a surface waveguide.

Rao and Hamid [5, 6] have investigated the effects of an intervening airgap on some propagation parameters of a circular surface waveguide. The proposed structure, shown in Fig. 1, consists of a central conducting rod surrounded by a dielectric layer and with an intervening airgap which they have called the modified Goubau line. Their first results show that an improvement of the attenuation and bandwidth can be achieved by the introduction of such an airgap.

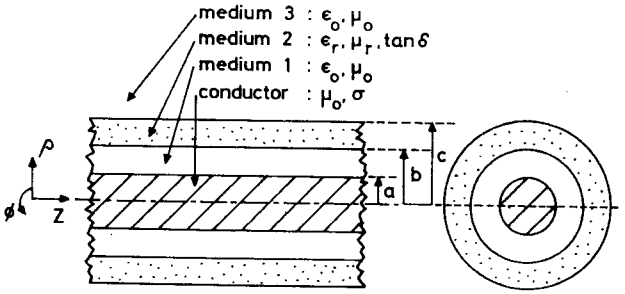

Fig. 1 *Geometry of the surface waveguide*

The suggested applications for such types of surface waveguides require single-mode propagation of the signal, but the proposed surface waveguide exhibits two fundamental modes with no cutoff frequency. Rao and Hamid [7] have derived an expression of the characteristic equation which gives rise to the whole spectrum of guided modes. Applying a surface impedance method [8], it has been demonstrated that this spectrum includes a hybrid mode with no cutoff frequency, in addition to the TM-mode previously reported [5]. So, using this waveguide, at least two guided modes will be present at any application.

We are concerned in showing the radial field structure and the propagation characteristics of both fundamental modes, as well as their dependence on the airgap and frequency. These results can help in the practical design of such guides, provided there is a good understanding of the differences between both modes, and can be useful in choosing the one which is more suitable for a given application, as well as avoiding the excitation and propagation of the other. The thickness of the airgap is a new parameter that might be used to improve the propagation characteristics of the surface waveguide as a low-loss transmission line, decreasing the attenuation without increasing the radius of the effective cross-section. This parameter can be also used to control the penetration of

Paper 4884H (E12) received 13th February 1986
The authors are with the Departamento de Electricidad y Magnetismo, Facultad de Fisica, Universidad de Valencia, Burjasot, Valencia, Spain

the fields in the surrounding medium, allowing a proper design of the waveguide as a leaky transmission line.

Different values of ε_r and μ_r have been computed, but we only show here the results corresponding to the case of polystyrene ($\varepsilon_r = 2.56$, $\mu_r = 1$). Other values give rise, typically, to the same qualitative behaviour of the propagation parameters of the surface waveguide.

2 Characteristic equation and low-frequency approximation

The application of the boundary-value technique to the circular surface waveguide shown in Fig. 1 yields the characteristic equation of the guided modes. This characteristic equation can be expressed as a determinant [9], the solution of which provides the values of the normalised transverse factors x and y:

$$\begin{vmatrix}
I_{na} & K_{na} & 0 & 0 & 0 & 0 & 0 & 0 & 0 & 0 \\
I_{nb} & K_{nb} & -J_{nb} & -Y_{nb} & 0 & 0 & 0 & 0 & 0 & 0 \\
\frac{I'_{nb}}{x} & \frac{K'_{nb}}{x} & \frac{\varepsilon_r}{y}J'_{nb} & \frac{\varepsilon_r}{y}Y'_{nb} & 0 & AI_{nb} & AK_{nb} & BJ_{nb} & BY_{nb} & 0 \\
0 & 0 & J_{nc} & Y_{nc} & -K_{nc} & 0 & 0 & 0 & 0 & 0 \\
0 & 0 & \frac{\varepsilon_r}{y}J'_{nc} & \frac{\varepsilon_r}{y}Y'_{nc} & \frac{K'_{nc}}{x} & 0 & 0 & DJ_{nc} & DY_{nc} & CK_{nc} \\
0 & 0 & 0 & 0 & 0 & I'_{na} & K'_{na} & 0 & 0 & 0 \\
0 & 0 & 0 & 0 & 0 & I_{nb} & K_{nb} & -J_{nb} & -Y_{nb} & 0 \\
AI_{nb} & AK_{nb} & BJ_{nb} & BY_{nb} & 0 & \frac{I'_{nb}}{x} & \frac{K'_{nb}}{x} & \frac{\mu_r}{y}J'_{nb} & \frac{\mu_r}{y}Y'_{nb} & 0 \\
0 & 0 & 0 & 0 & 0 & 0 & 0 & J_{nc} & Y_{nc} & -K_{nc} \\
0 & 0 & DJ_{nc} & DY_{nc} & CK_{nc} & 0 & 0 & \frac{\mu_r}{y}J'_{nc} & \frac{\mu_r Y'_{nc}}{y} & \frac{K'_{nc}}{x}
\end{vmatrix} = 0 \qquad (1)$$

The integer n fixes the angular dependence of the fields through the function $\exp(jn\phi)$. The sub-indices a, b and c are the values of ρ in the arguments of these functions. These arguments are $(y\rho/c)$ for the J_n and Y_n functions, and $(x\rho/c)$ for the I_n and K_n functions. The rest of the symbols are defined by

$$\begin{aligned}
x &= hc & h^2 &= \beta^2 - k_0^2 \\
y &= kc & k^2 &= k_0^2 \varepsilon_r \mu_r - \beta^2 \\
x^2 + y^2 &= f_0^2 & f_0 &= k_0 c\sqrt{\varepsilon_r \mu_r - 1}
\end{aligned} \qquad (2)$$

$$A = \frac{nc\beta}{x^2 bk_0} \qquad B = \frac{nc\beta}{y^2 bk_0} \qquad C = \frac{n\beta}{x^2 k_0} \qquad D = \frac{n\beta}{y^2 k_0}$$

The low-frequency approximation of the characteristic equation can be used to prove the existence of modes with no cutoff frequency. Previously [5], it has been proved that there exists a TM mode with no cutoff frequency, which is given by the approximation

$$x^2 \ln \frac{2b}{\Gamma x a} = \frac{y^2}{\varepsilon_r} \ln \frac{c}{b} \qquad (3)$$

Applying a surface impedance method [8], it is possible to rewrite the characteristic equation (eqn. 1) in a more convenient way in order to prove that it predicts another solution with no cutoff frequency. This second fundamental mode is a hybrid mode, and its low frequency approximation is given by the equation

$$\ln \frac{2}{\Gamma x} = \frac{F}{2y^2} \qquad (4)$$

where F is a postive factor which is a function of a, b, c, ε_r and μ_r [9].

The two modes with no cutoff frequency belong to the groups of symmetry $n = 0$ and $n = 1$. Following the nomenclature used by Zelby [10] and Semenov [11] for the Goubau line, the two fundamental modes will be named the TM_{00} and the EH_{10} modes.

These two equations, eqns. 3 and 4, are important by themselves because they prove the existence of two guided modes with no cutoff frequency, the two fundamental modes of this circular surface waveguide. At the same time, each is a low-frequency approximation of the characteristic equation for one of these modes, so they can provide a useful and easy way to obtain an approximated value of their propagation parameters. These approximations introduce, typically, a maximum error of 10% when the factor x is smaller than 1. The numerical results that are shown here have been all computed using eqn. 1.

A direct inspection of these low-frequency approximations provides a qualitative difference between the two fundamental modes. The TM_{00} mode will exhibit x- and y-factors of the same order of magnitude, except for very low frequencies, when the factor $\ln(2b/\Gamma xa)$ is large. These very low frequencies, typically of the order of 10 MHz, are clearly not of interest. However, the EH_{10}-mode will exhibit an x-factor which is much smaller than the y-factor. This qualitative difference has a lot of consequences which can be observed in the following Sections.

3 Transverse propagation factor x

In the external medium, which is the air that surrounds the guide, the radial dependence of the fields are fixed by the modified Bessel function $K_n(x\rho/c)$. Such a function provides the expected transversal decay, which can be approximated by an exponential of argument $(-x\rho/c)$. Therefore the transverse propagation factor x gives direct information about the radial decay of the fields in the external medium.

Fig. 2 shows two typical examples of the dependence of x on the relative thickness of the airgap. The radial decay of the fields decreases with an increase in the thickness of the airgap, which is the kind of result we would expect.

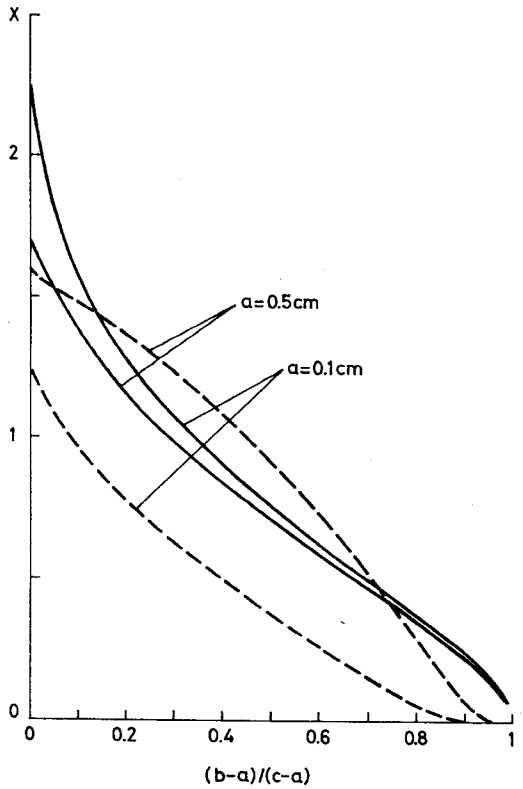

Fig. 2 *Radial propagation factor x as a function of* $(b-a)/(c-a)$
$c = 1$ cm, $\varepsilon_r = 2.56$, $\mu_r = 1$, $\lambda_0 = 3.2$ cm
——— TM_{00}
- - - - EH_{10}

4 Radius of the effective cross-section

Any practical application of a surface waveguide will ask for a knowledge of the minimum distance at which any external perturbation will produce a non-negligible effect on the guided signal. Such a distance can be defined in terms of the transverse propagation factor x, but this is insufficient and can produce quite misleading results. Indeed, a given value of the factor x can apply whether the contribution of the internal fields to the total Poynting vector flux is larger or smaller than the contribution of the external fields. In the first case, even with a small value of x, any external perturbation will not affect the propagation of the signal.

We have defined the radius of the effective cross-section (RECS) as the radius of the cross-section within which 90% of the Poynting vector flux takes place. Fig. 3 shows the values of RECS against the relative thickness of the airgap. We can observe that the RECS does not increase as we should expect from the decrease of the transverse propagation factor x (Fig. 2). For small values of the relative thickness of the airgap, when the factor x decreases strongly, the RECS remains, typically, below 2 cm. On the other hand, the RECS increases sharply only for relative large values of the thickness of the airgap.

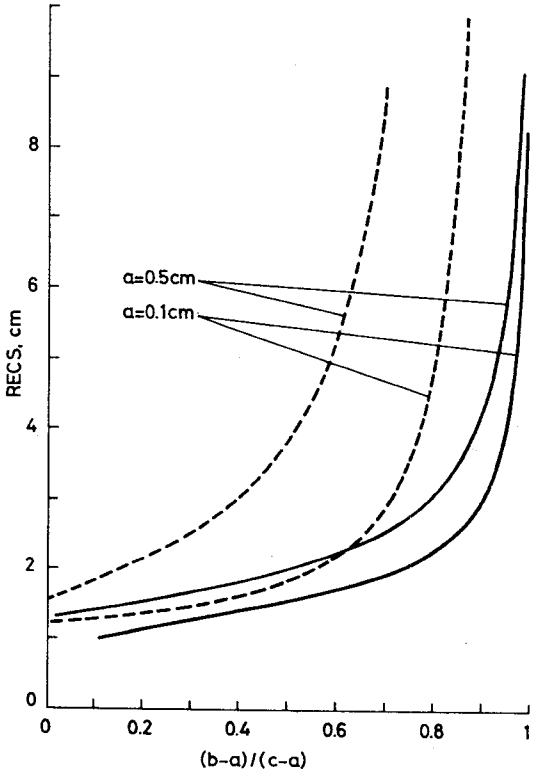

Fig. 3 *RECS as a function of* $(b-a)/(c-a)$
$c = 1$ cm, $\varepsilon_r = 2.56$, $\mu_r = 1$, $\lambda_0 = 3.2$ cm
——— TM_{00}
- - - - EH_{10}

Bearing in mind that the RECS provides more practical information than the factor x about the penetration of the fields in the external medium, Fig. 3 shows how this penetration can be controlled with the airgap. It is shown that, up to a certain value of the thickness of the airgap, this parameter can be used to modify the propagation characteristics of the waveguide preserving a small value of the RECS. For large values of the thickness of the airgap, a small change in it can broadly control the penetration of the fields in the external medium, and this can allow a proper design of the surface waveguide as a leaky transmission line.

5 Relative contributions to the power flow

We have found it very useful to evaluate the relative contributions of the fields within each medium to the total flux of the Poynting vector. These contributions P_1, P_2 and P_3 provide a good description of the way in which the introduction of the airgap modifies the radial field structure.

Fig. 4 shows that, with the introduction of the airgap, P_2 decreases, and P_1 and P_3 increase. Such redistribution of the fields is quite interesting because, for small values of the thickness of the airgap, as P_2 decreases, P_1 increases sharply and P_3 smoothly. And for large values, P_1 now decrease sharply and P_3 increases still more. These results are consistent with the previous two Sections.

6 Comparing the TM_{00} and EH_{10} modes

We are concerned in this section to show some qualitative differences between the two fundamental modes, which would provide useful information about which of these modes is more suitable for a given application.

Fig. 5 shows the relative contributions P_i as a function of the normalised frequency f_0. It is important to realise that, for this example, the interval of normalised frequencies [0, 3.6] is the interval within which the rest of the modes are below their cutoff frequencies. We can observe that, in this interval, the fields of the EH_{10} mode penetrate more deeply into the external medium.

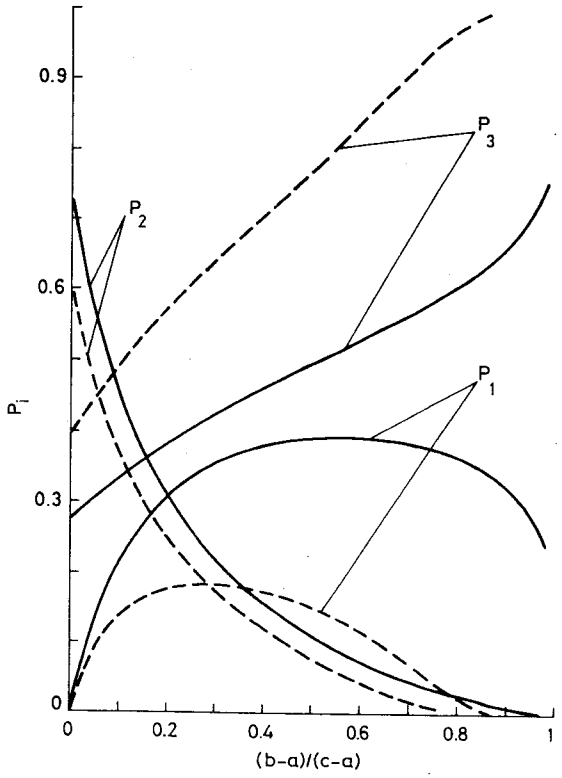

Fig. 4 P_1, P_2 and P_3 as a function of $(b-a)/(c-a)$
$c = 1$ cm, $a = 0.5$ cm, $\varepsilon_r = 2.56$, $\mu_r = 1$, $\lambda_0 = 3.2$ cm
——— TM_{00}
- - - - EH_{10}

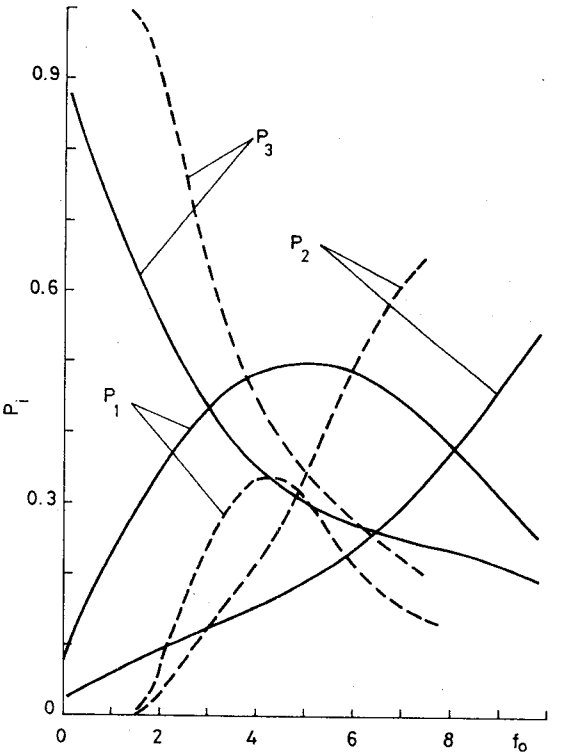

Fig. 5 P_1, P_2 and P_3 as a function of f_0
$c = 1$ cm, $a = 0.5$ cm, $b = 0.75$ cm, $\varepsilon_r = 2.56$, $\mu_r = 1$
——— TM_{00}
- - - - EH_{10}

Fig. 6 shows the values of the relative contributions P_i at a given RECS. This plot is interesting because it shows that the differences observed in Fig. 5 are probably due to the intrinsic structural differences between the two fundamental modes. When both modes exhibit the same RECS, but at different frequencies, the TM_{00} mode has a larger value of P_1 and a smaller value of P_2 than the EH_{10} mode, which will provide a smaller attenuation for the TM_{00} mode, as we will discuss in Section 8.

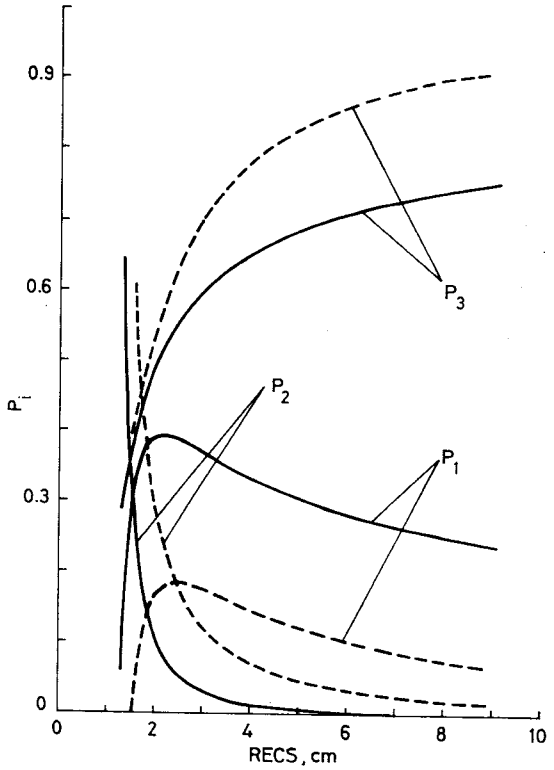

Fig. 6 P_1, P_2 and P_3 as a function of RECS
$c = 1$ cm, $a = 0.5$ cm, $b = 0.75$ cm, $\varepsilon_r = 2.56$, $\mu_r = 1$
——— TM_{00}
- - - - EH_{10}

7 Field patterns

The patterns of the transverse field components [12] provide graphical information about the intensity of the fields on a cross-section of the guide. This is quite useful for looking at the points of maximum intensity and to work out the kind of coupling we can expect with other guides or sources.

The surface impedance method [8] provides a straightforward numerical evaluation of the field components. Three different symbols are used to represent the transverse components of the fields as a function of their amplitudes. A double arrow is used when the amplitude is between the maximum and 1 dB smaller than the maximum. A single arrow represents the fields that have an amplitude between 1 dB and 3 dB smaller than the maximum. A short, single line corresponds to those fields in which the amplitude is between 3 dB and 10 dB smaller than the maximum. Finally, no symbol is plotted when the amplitude is more than 10 dB below the maximum.

The way in which such patterns are modified by the

introduction of the airgap provides a qualitative explanation of the different nature of the two fundamental modes. Fig. 7 shows that, when the dielectric medium

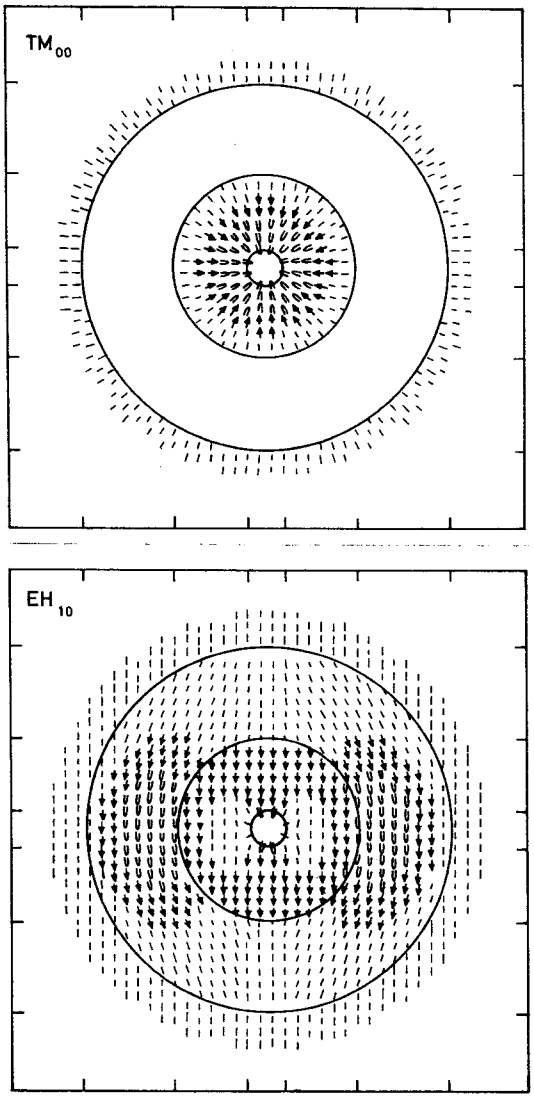

Fig. 7 *Transverse components of the electric field*
$c = 1$ cm, $a = 0.1$ cm, $b = 0.50$ cm, $\varepsilon_r = 2.56$, $\mu_r = 1$, $f_0 = 5$

and the conductor are separated by a thick airgap, the fields of the TM_{00}-mode look as if they are mainly attached to the surface of the central conducting rod, and that the fields of the EH_{10}-mode are mainly attached to the dielectric medium. This fact seems to relate the TM_{00}- and EH_{10}-modes with the fundamental symmetrical mode of the Sommerfeld line and with the fundamental hybrid mode of the circular dielectric waveguide. This idea looks to be consistent with the structure of the low-frequency approximations, eqns. 3 and 4, because both are very close to the low-frequency approximations of the fundamental modes of the Sommerfeld line [13] and the circular dielectric waveguide [14].

8 Attenuation

Taking into account the loss tangent of the dielectric medium and the finite conductivity of the conductor, the attenuation can be evaluated by means of a perturbative technique [9]. For a typical case of a surface waveguide made of a low-loss dielectric medium such as polystyrene ($\varepsilon_r = 2.56$, $\tan\delta = 0.0035$) and a good conductor such as copper, the main contribution to the attenuation factor are the losses in the dielectric medium α_d. Therefore we are concerned in this Section in showing only the calculated values of α_d.

Fig. 8 shows that the attenuation α_d can be improved by means of the introduction of an airgap. This is interesting because it means that an improvement can be achieved without increasing drastically the RECS (Fig. 3), at least for certain geometries of the surface waveguide.

Fig. 9 shows the same values of α_d but now plotted as a function of the RECS. We can observe clearly what was

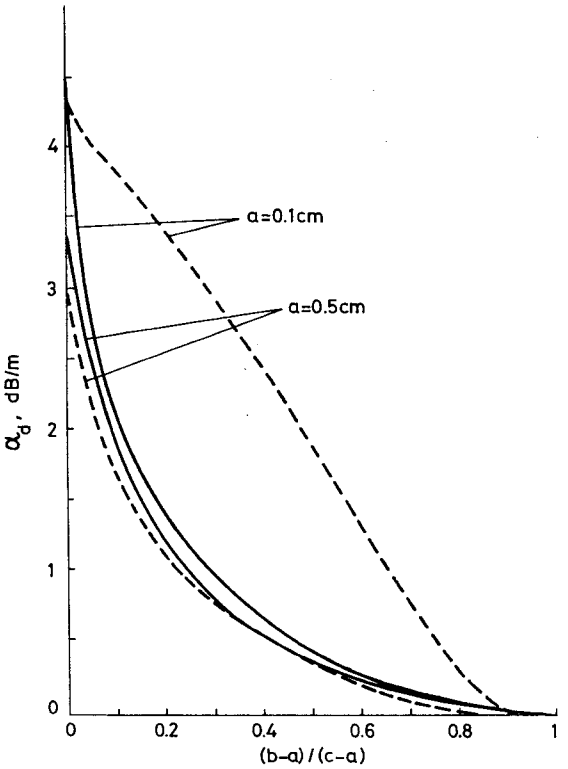

Fig. 8 *Attenuation factor α_d as a function of $(b-a)/(c-a)$*
$c = 1$ cm, $\varepsilon_r = 2.56$, $\mu_r = 1$, $\lambda_0 = 3.2$ cm
——— TM_{00}
- - - - EH_{10}

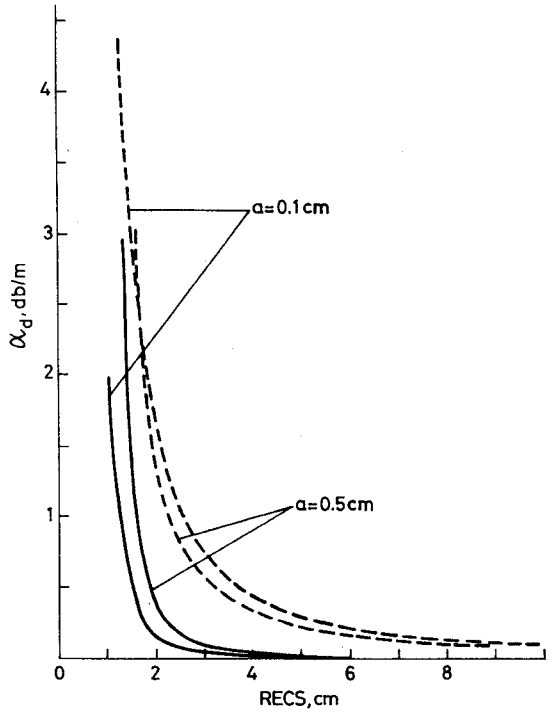

Fig. 9 *Attenuation factor α_d as a function of RECS*
$c = 1$ cm, $\varepsilon_r = 2.56$, $\mu_r = 1$, $\lambda_0 = 3.2$ cm
——— TM_{00}
- - - - EH_{10}

suggested in Section 6. The more advantageous distribution of the Poynting vector flux of the TM_{00}-mode gives rise to a smaller attenuation factor at a given RECS.

9 Conclusion

The main effects produced by the introduction of an intervening airgap in a circular surface waveguide have been discussed. It has been shown how the airgap modifies the radial field structure and the propagation characteristics of the two fundamental modes. It is possible to decrease the attenuation without increasing drastically the radius of the effective cross-section, and it is possible to control the penetration of the fields into the external medium with a small change in the thickness of the airgap.

10 References

1 BARLOW, H.M.: 'Low-loss waveguides', Conference of the URSI 16th General Assembly, Ottawa, Canada, 1969, p. 71
2 OLINER, A.A.: 'A new class of reactive wall waveguide for low-loss applications', Conference Abstracts of the URSI 16th General Assembly, Ottawa, Canada, 1969, pp. 72–73
3 TOWAIJ, S.J., and HAMID, M.A.K.: 'Difraction by a multilayered dielectric coated sphere with an azimuthal slot', *Proc. IEE*, 1971, **118**, pp. 1209–1214
4 RAO, T.C.K., and HAMID, M.A.K.: 'Scattering by a multilayered dielectric coated conducting cylinder', *Int. J. Electron.*, 1975, **38**, pp. 667–673
5 RAO, T.C.K., and HAMID, M.A.K.: 'Propagation characteristics of a dielectric-coated conducting surface-wave transmission line with an intervening airgap', *Proc. IEE*, 1976, **123**, pp. 973–980
6 RAO, T.C.K., and HAMID, M.A.K.: 'Frequency bandwidth of the modified Goubau line', *ibid.*, 1977, **124**, pp. 1017–1018
7 RAO, T.C.K., and HAMID, M.A.K.: 'Mode spectrum of the modified Goubau line', *ibid.*, 1979, **126**, pp. 1227–1232
8 ANDRES, M., and SUCH, V.: 'Surface impedance method applied to the modified Goubau line', IEEE Mediterranean Electrotechnical Conf., Madrid, Spain, 1985, V-III, pp. 105–108
9 ANDRES, M.: 'Estudio de la Linea de Goubau Modificada', Ph.D. Thesis, Dept. of Electricity and Magnetism, University of Valencia, Spain, April 1985
10 ZELBY, L.W.: 'Propagation modes in a dielectric coated wire', *J. Franklin Inst.*, 1962, **274**, pp. 85–97
11 SEMENOV, N.A.: 'Wave modes in a surface wave line', *Radio Eng. Electron. Phys.*, 1964, **9**, pp. 989–995
12 KAJFEZ, D.: 'Modal field patterns in dielectric rod waveguides', *Microwave J.*, 1983, **25**, pp. 181–192
13 GOUBAU, G.: 'Surface waves and their application to transmission lines', *J. Appl. Phys.*, 1950, **21**, pp. 1119–1128
14 SUCH, V., and ANDRES, M.: 'Calculo de los parametros caracteristicos de una guia dielectrica cilindrica a partir de la solución de la ecuación caracteristica compleja', URSI I Symp. Nacional, Spain, Madrid, 1980, pp. 15–19